DOI 10.1007/s10946-016-9574-8
Journal of Russian Laser Research, Volume 37, Number 3, May, 2016

COHERENT EXCITATION OF SODIUM CHLORIDE NANOPARTICLES

H. V. Ehrlich,[1] A. D. Kudryavtseva,[2*] G. V. Lisichkin,[1] T. V. Mironova,[2] V. V. Savranskii,[3] N. V. Tcherniega,[2] K. I. Zemskov,[2] and M. P. Zhilenko[1]

[1] *Department of Chemistry, Lomonosov Moscow State University Vorob'evy Gory, Moscow 119992, Russia*

[2] *Lebedev Physical Institute, Russian Academy of Sciences Leninskii Prospect 53, Moscow 119991, Russia*

[3] *Prokhorov General Physics Institute, Russian Academy of Sciences Vavilova Street 38, Moscow 119991, Russia*

*Corresponding author e-mail: akudr@sci.lebedev.ru

Abstract

We register stimulated low-frequency Raman scattering (SLFRS) caused by laser-pulse interaction with nanoparticle acoustic vibrations in an ethanol suspension of sodium chloride nanoparticles and measure the SLFRS conversion efficiency and threshold. Frequency shifts of scattered light from the exciting light frequency are situated in the gigahertz range. We show that the frequency shifts increase with decrease in the nanoparticle sizes.

Keywords: nanoparticles, laser, stimulated scattering, vibrations.

1. Introduction

Nanoparticles play an increasing role not only in scientific investigations, but also in industry, medicine, and biology. They are used for different purposes in industrial processes. Thus, it is important to study different systems containing nanoparticles and develop methods for their characterization. Low frequency Raman scattering (LFRS) is a powerful tool for investigating nanoparticle properties. Each nanoparticle has a set of natural acoustic frequencies determined by its morphology. Some nanoparticle vibration eigenmodes obeying the Raman selection rules may appear in the LFRS spectra. The frequency shifts of Stokes and anti-Stokes LFRS components are in the terahertz or gigahertz range and are determined by the shape of nanoparticles, their sizes, and elastic properties [1]. The line width of scattered light is defined by the homogeneous broadening due to the interaction with surrounding media and the inhomogeneous broadening due to the particle-size distribution [2]. So, analysis of the LFRS spectral characteristic can provide important information on the physical properties of the nanoparticles and the properties of the surrounding environment.

Recently, it has been shown that, in different systems consisting of nanoparticles of various nature, a stimulated analog of the LFRS can be excited [3, 4]. The SLFRS was observed in different materials: highly-ordered samples such as opal matrices and nanocomposites based on them, nanostructured thin films, and disordered materials such as suspensions of different nanoparticles (metals, semiconductors, dielectrics) [5, 6].

Manuscript submitted by the authors in English on April 20, 2016.

The high efficiency of SLFRS conversion is evidence of intense coherent nanoparticle oscillations at terahertz or gigahertz frequencies. The precise frequency is determined by the characteristics of the nanoparticles and environment. The coherent phonon excitation at THz or GHz frequencies can lead to many practical applications and, from this point of view, the experimental SLFRS observation in different systems is of great practical importance.

Among a large number of nanoparticles, some may exist in nature, for instance, NaCl nanoparticles may appear in aerosols of sea evaporations [7, 8]. They can take part in cloud formation, interact with inorganic and organic materials existing at the same time in the atmosphere, and even influence the ozone level [9–11]. Also NaCl nanoparticles can play an important role in some processes in biology and medicine; for instance, in tissue engineering [12]. Some methods of preparing NaCl nanoparticles have been described in the literature, as well as their properties especially connected with such atmospheric phenomena as deliquescence and efflorescence [13]. Deliquescence is transformation of crystalline NaCl nanoparticles into aqueous saline droplets, and efflorescence is the inverse process of water evaporation and drying of nanoparticles.

The size distribution of polydisperse and monodisperse NaCl nanoparticles as a function of temperature was studied in [14]. In [15], the methods of nanoparticle embedding into polymer and glass substrates have been described. The morphology and structure of coatings (in particular, NaCl) were characterized by different methods such as X-ray diffraction (XRD), Raman scattering, and luminescence. The NaCl-nanoparticle fragmentation under the action of UV laser radiation was studied in [16].

Atmospheric NaCl nanoparticles contain water, usually as a layer covering the particle. In this paper, we produce and study NaCl nanoparticles that do not contain water. For this purpose, we use NaCl nanoparticle suspensions in ethanol, which practically does not dissolve NaCl. We investigate stimulated low-frequency Raman scattering (SLFRS) appearing in the NaCl nanoparticle suspension under the action of nanosecond laser pulses.

2. Preparation and Characterization of Nanoparticles

NaCl powders are obtained by different methods. The samples of NaCl (Nos. 1 and 3) were obtained in the reaction of sodium diethylmalonate with acetyl chloride in toluene. If the reaction was carried out at room temperature, yellowish crystals of NaCl (No. 1) were obtained. If sodium diethylmalonate in toluene was cooled to 17–18°C before adding acetyl chloride, white crystals of NaCl (No. 3) were formed. The NaCl sample (No. 2) was formed when chloroform and metal sodium were mixed in ethanol under cooling at 17–18°C. Lastly, the NaCl powder (No. 4) was obtained in the reaction of sodium acetate with acetyl chloride in ethanol under stirring and cooling at 17–18°C. All organic components of reactions and organic solvents were previously dried and distilled, that is, they are free of water.

To determine the average size of elementary NaCl particles, we employed phase analysis. It was carried out on a Stoe Stad P power diffractometer in the θ/θ geometry using CuK α radiation. The samples were studied in the 25–50° range with an increment of 0.05° and an exposure to a dot of 10 s. The result is presented in Fig. 1.

We used the approximation method based on the analysis of the integral width of diffraction maxima to determine the mean size D of the coherent scattering region (CSR). The diffraction maximum (200) with an increment of 0.05° and time of 50 s per dot was used to estimate the CSR of NaCl.

We used the Scherrer equation for the CSR calculation:

$$\Delta(2\theta)\ (\text{rad}) \approx 0.94\,\lambda/\text{D}\cos\theta,$$

where $\Delta(2\theta)$ is the full width at half-maximum (FWHM) of the peak (radians) corrected for instrumental broadening, λ is the wavelength of X-rays (Å), and D is the mean size of the coherent scattering region.

In accordance with the data of X-ray phase analysis, the four NaCl samples (Nos. 1, 2, 3, and 4) have a mean size of the CSR equal to 41.6, 46.0, 52.0, and 59.6 nm, respectively.

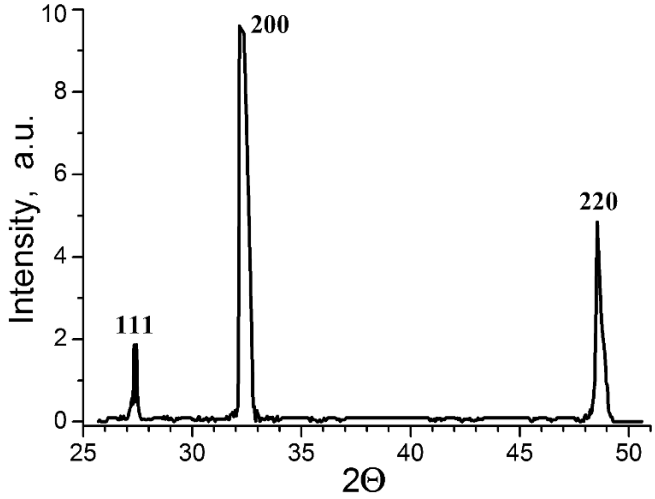

Fig. 1. Typical diffractogram of sodium chloride powder where only peaks of NaCl are visible.

3. Experimental

The experimental setup for SLFRS investigations in NaCl nanoparticle suspensions is shown in Fig. 2.

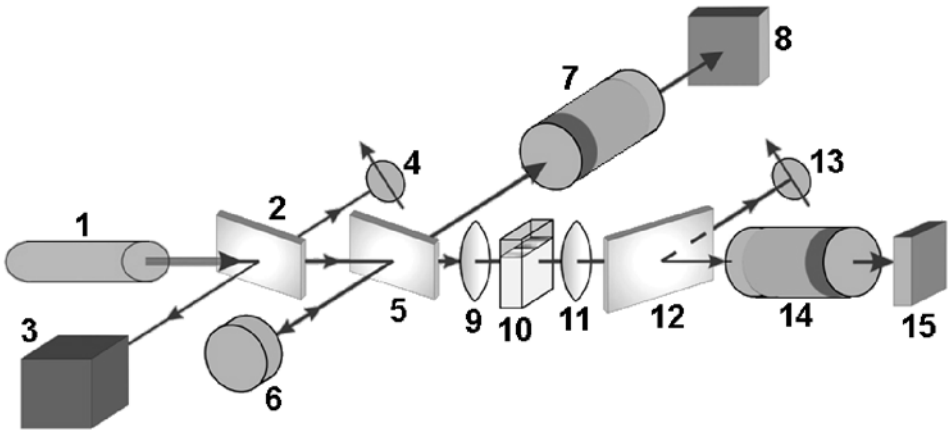

Fig. 2. Experimental setup with ruby laser 1, glass plates 2, 5, and 12, measurement system for laser pulse characteristics 3, systems for measuring the SLFRS energy in forward 4 and backward 13 directions, mirror 6, Fabry–Pérot interferometers 7 and 14, photo cameras registering the SLFRS spectra 8 and 15, lenses 9 and 11, and quartz cell 10.

Scattering was excited by single pulses of ruby laser (λ = 694.3 nm, τ = 20 ns, $E_{\max}$ = 0.3 J, $\Delta\nu$ = 0.015 cm^{-1}, and divergence $3.5 \cdot 10^{-4}$ rad). The laser light was focused in the center of a 1 cm quartz cell with NaCl suspension. Lenses with a focal length of 10, 5, and 3 cm were used for focusing the laser light. This provides the possibility to expand the range of the laser intensity for the SLFRS excitation. The SLFRS spectra were registered by Fabry–Pérot interferometers with a range of dispersion of 1.67 cm^{-1}.

At an input laser pulse intensity exceeding a certain threshold, the SLFRS propagating in the forward and backward directions was registered. We observed the SLFRS in ethanol suspensions containing NaCl nanoparticles of different sizes. In all cases, with the help of Fabry–Pérot interferometers, we observed

additional rings corresponding to the scattered light in the spectra obtained. We observed the scattering in both backward and forward directions approximately at the same threshold. The line width and divergence of the SLFRS were close to the corresponding values of the exciting laser light. In Fig. 3, we show two spectra of the light propagating through a cell with NaCl suspension (No. 4). Figure 3 a corresponds to a laser intensity of 0.01 GW/cm^2 (below the threshold), and Fig. 3 b corresponds to a laser intensity of 0.09 GW/cm^2 (above the threshold).

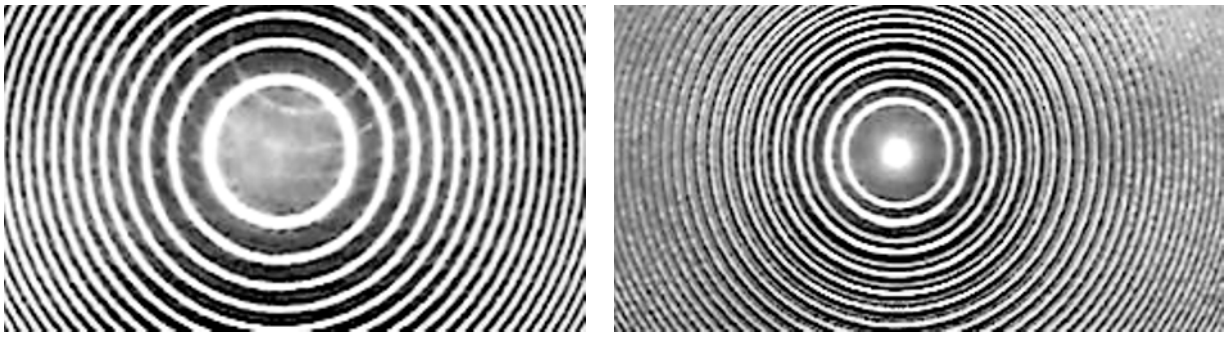

Fig. 3. Spectrum of the laser light (a) and spectrum of the laser light and SLFRS (b). The dispersion range is equal to 1.67 cm^{-1}.

The frequency shifts of the SLFRS correspond to the eigenvalues of nanoparticle acoustic vibrations in the GHz range. We measured the SLFRS frequency shifts for NaCl nanoparticles of different sizes. In Table 1, we present the maximum conversion efficiency η, SLFRS thresholds P, SLFRS frequency shifts $\Delta\nu$, and the values of the NaCl nanoparticles coherent scattering region D for the samples under investigation.

Assuming the size of the coherent scattering region to be close to the size of nanoparticles, we determine the frequency shift. The frequency shifts appeared to be proportional to $1/D$, where D is the size of the nanoparticle coherent scattering region; the results are shown in Fig. 4.

In [3,6], we reported an increase in the SLFRS frequency shift with decrease in the nanoparticle sizes in different materials [3, 6]. This is a manifestation of the fact that the oscillation frequency ν of a free nanoparticle is proportional to the orientationally averaged speed of the sound v in the nanoparticle and inversely proportional to its characteristic size D, i.e., $\nu \sim v/D$.

Table 1. SLFRS Characteristics for the NaCl Nanoparticle Suspension in Ethanol.

Sample	η %	P GW/cm^2	$\Delta\nu$ GHz	D nm
1	8	0.1	33.0	41.6
2	8	0.08	23.4	46.0
3	9	0.08	21.9	52.0
4	11	0.07	15.0	59.6

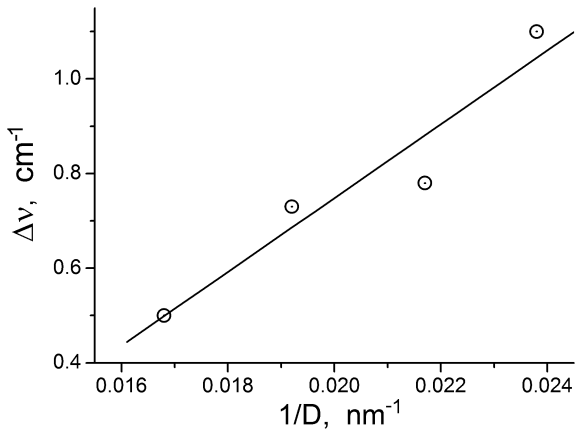

Fig. 4. Frequency shifts of the SLFRS components in NaCl nanoparticles in ethanol.

4. Summary

The physical mechanism of SLFRS excitation is nearly the same as for stimulated Raman scattering in transparent solids and liquids and can be briefly described as follows [17]. The electromagnetic laser field induces the polarization of the nanoparticles, which are vibrating with their eigenfrequency. This polarization is a source of inelastically scattered wave. When the laser intensity exceeds the threshold value, the initial spontaneously scattered light can enhance further scattering of the incident wave and lead to an effective growth of the total scattered light. This scattering caused by the initially scattered light is called the stimulated scattering. The interaction of both waves produces a force of the form $\sim \left(\frac{d\alpha}{dq}\right)_{ij} E_i E_j$, where α is the nanoparticle polarizability and q is a vibrational coordinate. This mechanical force coherently excites Raman-active vibrational modes of the nanoparticles. There is one more force defined by the interaction of the induced dipole moments of neighboring nanoparticles. This additional force is proportional to the nanoparticle polarizabilities and inversely proportional to the cube of the distance between the nanoparticles and must be taken into consideration in the case of close-packed nanoparticle systems. High SLFRS conversion efficiency is evidence of effective coherent excitation of nanoparticle vibrations. The maximum intensity value that can be transformed into acoustic excitation of nanoparticles is defined by the nanoparticle eigenfrequency and the laser wave's frequency ratio and is $\sim 10^{-4}$ of the laser intensity.

The SLFRS excitation provides the generation of the light field consisting of two waves – laser and SLFRS, nearby intensity and wavelength. The frequency shift between them depends on the nanoparticle dimensions and material properties; thus, one can control the change in its value. This fact provides the possibility to create a source of biharmonic pumping, which can be used in basic research, as well as in many applications in nonlinear spectroscopy, particularly, for the investigation of systems with eigenfrequencies in gigahertz and terahertz ranges.

In biology and medicine, biharmonic pumping may be used for the impact on biologic nano-objects and for their identification (for instance, some viruses are known to be of spherical or cylindrical shape with a size of the order of 100 nm). Due to short pulse durations, the SLFRS can be applied for determination of the nanoparticle size in real time, for instance, in aerosols.

References

1. E. Duval, A. Boukenter, and B. Champagnon, *Phys. Rev. Lett.*, **56**, 2052 (1986).
2. M. Ivanda, K. Babocsi, C. Dem, et al., *Phys. Rev. B*, **67**, 235329 (2003).
3. N. V. Tcherniega, M. I. Samoylovich, A. D. Kudryavtseva, et al., *Opt. Lett.*, **35**, 300 (2010).
4. N. V. Tcherniega, K. I. Zemskov, V. V. Savranskii, et al., *Opt. Lett.*, **38**, 824 (2013).
5. N. V. Tcherniega and A. D. Kudryavtseva, *J. Surf. Invest.: X-Ray, Synchrotron Neutron Technol.*, **3**, 513 (2009).
6. A. D. Kudryavtseva, N. V. Tcherniega, M. I. Samoylovich, and A. S. Shevchuk, *Int. J. Thermophys.*, **33**, 2194 (2012).
7. R. Bahadur and L. Russel, *J. Chem. Phys.*, **129**, 094508 (2008).
8. L. M. Russel and Y. Ming, *J. Chem. Phys.*, **116**, 311 (2002).
9. P. J. Adams, J. H. Seinfeld, D. Koch, et al., *J. Geophys. Res.*, **106**, 1097 (2001).

10. N. L. Prisle, T. Raatikainen, A. Laaksonen, and M. Bilde, *Atm. Chem. Phys.*, **10**, 5663 (2010).
11. B. J. Finlayson-Pitts and J. C. Hemminger, *J. Phys. Chem. A*, **104**, 11463 (2000).
12. F. A. Landis, J. S. Stephens, J. A. Cooper, et al., *Biomacromol.*, **7**, 1751 (2006).
13. G. Biskos, A. Malinowski, L. Russell, et al., *Aerosol Sci. Technol.*, **40**, 97 (2006).
14. T. M. Chen and H. M. Chein, *Aerosol Air Quality Res.*, **6**, 305 (2006).
15. S. Kiel, O. Grinberg, N. Perkas, et al., *Beilstein J. Nanotechnol.*, **3**, 267 (2012).
16. J. H. Choi, C. B. Stipe, C. P. Koshland, et al., *J. Appl. Phys.*, **97**, 124315 (2005).
17. Y. R. Shen and N. Blombergen, *Phys. Rev. A*, **137**, 1787 (1965).